

Small-angle neutron scattering (SANS) and spinecho SANS measurements reveal the logarithmic fractal structure of the large-scale chromatin organization in HeLa nuclei

Iashina, Ekaterina G.; Filatov, Mikhail V.; Pantina, Rimma A.; Varfolomeeva, Elena Y.; Bouwman, Wim G.; Duif, Chris P.; Honecker, Dirk; Pipich, Vitaliy; Grigoriev, Sergey V.

DOI

[10.1107/S160057671900921X](https://doi.org/10.1107/S160057671900921X)

Publication date

2019

Document Version

Final published version

Published in

Journal of Applied Crystallography

Citation (APA)

Iashina, E. G., Filatov, M. V., Pantina, R. A., Varfolomeeva, E. Y., Bouwman, W. G., Duif, C. P., Honecker, D., Pipich, V., & Grigoriev, S. V. (2019). Small-angle neutron scattering (SANS) and spinecho SANS measurements reveal the logarithmic fractal structure of the large-scale chromatin organization in HeLa nuclei. *Journal of Applied Crystallography*, 52(4), 844-853. <https://doi.org/10.1107/S160057671900921X>

Important note

To cite this publication, please use the final published version (if applicable).
Please check the document version above.

Copyright

Other than for strictly personal use, it is not permitted to download, forward or distribute the text or part of it, without the consent of the author(s) and/or copyright holder(s), unless the work is under an open content license such as Creative Commons.

Takedown policy

Please contact us and provide details if you believe this document breaches copyrights.
We will remove access to the work immediately and investigate your claim.



Small-angle neutron scattering (SANS) and spin-echo SANS measurements reveal the logarithmic fractal structure of the large-scale chromatin organization in HeLa nuclei

Ekaterina G. Iashina,^{a,b*} Mikhail V. Filatov,^b Rimma A. Pantina,^b Elena Yu. Varfolomeeva,^b Wim G. Bouwman,^c Chris P. Duif,^c Dirk Honecker,^d Vitaliy Pipich^e and Sergey V. Grigoriev^{a,b}

Received 15 March 2019

Accepted 27 June 2019

Edited by D. I. Svergun, European Molecular Biology Laboratory, Hamburg, Germany

Keywords: small-angle neutron scattering; spin-echo small-angle neutron scattering; fractals; chromatin; DNA.

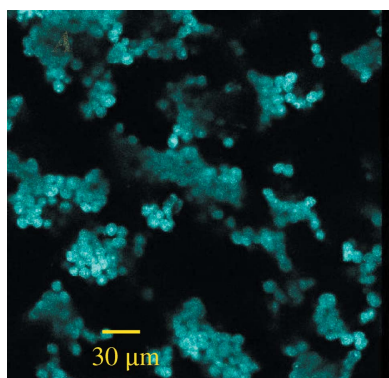
^aSaint Petersburg State University, Ulyanovskaya 1, Saint Petersburg, 198504, Russian Federation, ^bPetersburg Nuclear Physics Institute NRC ‘Kurchatov Institute’, Gatchina, Saint Petersburg, 188300, Russian Federation, ^cDelft University of Technology, Mekelweg 15, 2629 JB Delft, The Netherlands, ^dInstitut Laue–Langevin, F-38042 Cedex 9, Grenoble, France, and ^eHeinz Maier-Leibnitz Zentrum, Lichtenbergstrasse 1, 85747 Garching, Germany. *Correspondence e-mail: yashina_91@inbox.ru

This paper reports on the two-scale fractal structure of chromatin organization in the nucleus of the HeLa cell. Two neutron scattering methods, small-angle neutron scattering (SANS) and spin-echo SANS, are used to unambiguously identify the large-scale structure as being a logarithmic fractal with the correlation function $\gamma(r) \sim \ln(r/\xi)$. The smaller-scale structural level is shown to be a volume fractal with dimension $D_F = 2.41$. By definition, the volume fractal is self-similar at different scales, while the logarithmic fractal is hierarchically changed upon scaling. As a result, the logarithmic fractal is more compact than the volume fractal but still has a rather high surface area, which provides accessibility at all length scales. Apparently such bi-fractal chromatin organization is the result of an evolutionary process of optimizing the compactness and accessibility of gene packing. As they are in a water solution, the HeLa nuclei tend to agglomerate over time. The large-scale logarithmic fractal structure of chromatin provides the HeLa nucleus with the possibility of penetrating deeply into the adjacent nucleus during the agglomeration process. The interpenetration phenomenon of the HeLa nuclei shows that the chromatin-free space of one nucleus is not negligible but is as large as the volume occupied by chromatin itself. It is speculated that it is the logarithmic fractal architecture of chromatin that provides a comfortable compartment for this most important function of the cell.

1. Introduction

Speculations as to how DNA molecules a few metres long are packed inside a micrometre-sized nucleus have become the subject of textbooks (Alberts, 2008; Wolffe, 1999; Blossey, 2017). Even more hypotheses and experimental facts can be found in scientific papers (Misteli, 2007; Bintu *et al.*, 2012; Almassalha *et al.*, 2017; Yi *et al.*, 2015; Bénichou *et al.*, 2011; Joti *et al.*, 2012; Ou *et al.*, 2017; Widom & Klug, 1985; Woodcock *et al.*, 1993; Boettiger *et al.*, 2016; Grosberg *et al.*, 1988, 1993; Lieberman-Aiden *et al.*, 2009; Mirny, 2011), demonstrating that no consensus has been achieved and discussion on this subject is far from at an end. The concept of the fractal organization of chromatin appears to be one of the most productive hypotheses, but it is not well established yet.

A typical eukaryotic cell spends most of its lifetime in the interphase, with the chromatin distributed throughout the



nucleus forming a fractal architecture instead of chromosomes. It is the metabolic phase of the cell cycle when the cell acquires nutrients, creates and uses proteins and other molecules, and starts the process of its division by replicating the DNA. Moreover, the cell needs to carry out unpacking of the DNA and find a specific gene site in a short time. As was recently shown (Almassalha *et al.*, 2017; Misteli, 2007; Bintu *et al.*, 2012; Bénichou *et al.*, 2011; Yi *et al.*, 2015), the chromatin physical topology and gene expression are closely related. The fractal organization of chromatin can facilitate diffusion of proteins and thus can speed up the search for a target site (Bénichou *et al.*, 2011). Moreover, changing the fractal dimension of the chromatin structure on the nano-scale influences the transcriptional gene activation (Almassalha *et al.*, 2017). Thus, fractal DNA packing plays an important role in gene expression and epigenetic repression.

Obviously, to achieve the extreme density of the DNA packing and high accessibility of enzymes to a specific gene site, chromatin cannot be randomly distributed or fully disordered. Chromatin demonstrates a hierarchical structure that includes several organization levels (Bancaud *et al.*, 2012). The small-scale chromatin organization is well understood: nucleic acids build a double-helix DNA sequence which is complexed with histones to form nucleosomes. Each nucleosome consists of eight histone proteins around which the DNA wraps 1.5 times (Alberts, 2008). The organization of chromatin on a larger scale is the subject of debate. The supposition that nucleosomes fold up to produce a 30 nm fibre appeared to be an artefact of electron microscopy preparation (Ou *et al.*, 2017). Furthermore, the model of a crumpled or fractal globule (Grosberg *et al.*, 1988, 1993; Lieberman-Aiden *et al.*, 2009; Mirny, 2011; Boettiger *et al.*, 2016) proposed to describe the 3D configuration of chromatin does not satisfy all accumulated knowledge and in some cases clearly contradicts the experimental facts.

The model of a crumpled (fractal) globule comes from the investigation of interactions between genes by the Hi-C method, which is the modern derivative of the chromosome conformation capture (3C) method (Dekker *et al.*, 2002). The 3C method and its various derivatives (4C, 5C, Hi-C) measure the probability of an interaction between two regions of the genome in a large (10^5 – 10^6) cell population. While it is undeniable that these methods are effective in studying DNA packaging, they have some disadvantages as well (Lajoie *et al.*, 2015). The most significant drawback is related to the fact that the Hi-C method detects the frequency of an interaction between genes but not the distance. The formaldehyde cross-links will be only between genes which physically interact. Therefore, assumptions are needed about the relationship between physical distances and interaction frequencies, providing indirect methods for reconstructing the spatial density distribution of chromatin.

The model of the crumpled (fractal) globule represents a 3D polymer conformation, which is maximally compact and knot free. Its fractal architecture has often been illustrated by the 3D Hilbert curve with the claim that its fractal dimension is equal to 3. However, this illustration is misleading since the

most compact packing of the 3D Hilbert curve produces countless obstacles for enzymes getting to the specific gene site and thus makes these sites inaccessible. Moreover, as it is the curve with the densest and most homogeneous filling of the 3D space, the Hilbert curve is not a fractal object in its direct sense (Mandelbrot, 1983).

Small-angle scattering of neutrons or X-rays is probably the most informative and direct way to study the spatial distribution of chromatin density on the nano- and micro-scales. This method is actively used in various branches of science and technology, including condensed-matter physics, molecular biology, biophysics, polymer science and metallurgy (Bale & Schmidt, 1984; Martin & Hurd, 1987; Teixeira, 1988). The scattering intensity $I(Q)$ measured by this method is related to fluctuations in the scattering density $\rho(r)$ and is equal to the Fourier transform of the correlation function of the object $\gamma(r)$. The self-similarity of a fractal object is converted to a power law of the scattering intensity (Bale & Schmidt, 1984; Martin & Hurd, 1987; Teixeira, 1988). For example, a small-angle scattering experiment would show that the scattering intensity from the 3D Hilbert curve is described by the power law Q^{-D} with the exponent $D = 4$ (non-fractal volume particle), which is drastically different from the one obtained from the chromatin packed in the cell nucleus.

Experiments on the nuclei of chicken erythrocytes using small-angle neutron scattering (SANS) have shown a bifractal structure of the chromatin organization (Lebedev *et al.*, 2005; Iashina *et al.*, 2017). A power dependence of the scattering intensity with the exponent $D = 2.46 \pm 0.01$ was found in the momentum transfer range $[10^{-2} - 2.5 \times 10^0] \text{ nm}^{-1}$. In the frame of the fractal concept, $D = 2.46$ corresponds to a volume (mass) fractal with the fractal dimension $D_F = 2.46$. Its correlation function is described by the power function $\gamma(r) \sim (r/\xi)^{D_F-3}$ for $r < \xi$, where ξ is the size of the fractal. One of the most illustrative example objects with fractal dimension $D_F = 2.4$ is the diffusion-limited aggregation (DLA) cluster. A DLA cluster (also known as a Brownian tree) is a fractal aggregate where the shape of the cluster is controlled by the possibility of particles reaching the cluster via Brownian motion (Feder *et al.*, 1998).

Moreover, SANS experiments have revealed the existence of yet another fractal with a cubic dependence of the scattering intensity Q^{-3} in the range of momentum transfer $Q \in [3 \times 10^{-3} - 10^{-2}] \text{ nm}^{-1}$ (Iashina *et al.*, 2017). Independent spin-echo SANS (SESANS) measurements demonstrated that the spin-echo function is well described by the exponential law at a distance range of $[3 \times 10^2 - 10^4] \text{ nm}$. Both experimental dependencies reflect the nature of the structural organization of chromatin in the nucleus of a cell, which corresponds to the correlation function $\gamma(r) \sim \ln(\xi/r)$ for $r < \xi$, where $\xi = (3.69 \pm 0.07) \times 10^3 \text{ nm}$ is the size of the nucleus. On the basis of SANS and SESANS experiments on the chicken erythrocyte nuclei, we proposed a new model of the logarithmic fractal describing the large-scale chromatin organization in the interphase nucleus (Iashina *et al.*, 2017). It has the extraordinary scaling property $\gamma(r/a) = \gamma(r) + \ln(a)$, which can be formulated as follows: the scaling down by a gives an additive

constant to the correlation function, which distinguishes it from the regular fractal characterized by a multiplicative constant.

The available experimental data provide a complex picture of bi-fractality with reference to chromatin within the nucleus. From the point of view of the scattering contrast, both types of fractal architecture are built by the same material (chromatin) on a background of the heavy water used in the experiment. This picture can be inverted and the scattering is seen as one related to the chromatin-free space, *i.e.* as a net being built for the diffusive movement (Bancaud *et al.*, 2012). Therefore, different physical mechanisms for diffusion should be related to fractal architectures at the nano- and submicro-scales. Though the mass fractal dimension cannot be linked to the specific geometry, the model of the logarithmic fractal is rather unusual and is formed under the influence of two factors: maximization of the surface area (accessibility) and minimization of volume (compactness) (West *et al.*, 1999; Iashina *et al.*, 2017). The maximal possible area contributes to diffusive processes or target-search mechanisms of nuclear proteins such as transcription factors. On the other hand, the logarithmic fractal is more compact than any volume fractal and, therefore, the efficiency of interactions between distant genomic loci is increased on account of decreasing the distance between them (Iashina *et al.*, 2017; Iashina & Grigoriev, 2017). As to the fractal structure at smaller scales, the volume fractal architecture with the DLA model promotes the diffusive movement in chromatin-free space (accessibility) more than the compactness of the structure (Bancaud *et al.*, 2012).

In order to prove the concept of the bi-fractal structure of DNA organization for a wide variety of living cells, we applied the two experimental methods SANS and SESANS to study chromatin organization in the nucleus of the HeLa cell. The HeLa cell was chosen as it is a rapidly dividing active cell (Migliani, 2006), in contrast to the chicken erythrocyte nucleus which is synthetically inactive, *i.e.* it makes no DNA and no RNA and its chromatin is tightly condensed. The question arises: what are the similarities and differences in chromatin organization between dormant nuclei and active nuclei?

Recently, the large-scale organization of interphase chromatin in HeLa nuclei was studied by the ultra-small-angle X-ray scattering method in the momentum transfer range [3×10^{-3} – 3×10^{-2}] nm^{-1} (Joti *et al.*, 2012). To interpret the experimental result the authors used a model of an infinite surface fractal. It was shown that the scattering intensity obeys the power law $I(Q) \sim Q^{-D}$ with $D = 3.36$, suggesting that chromatin exhibits a fractal nature of genome organization. Unfortunately, the model used by the authors did not take into consideration the finite size of nuclei which cannot be neglected in this range of Q . In contrast, we consider the nucleus as being a finite fractal object since the scattering on scales close to the size of the nuclei changes the exponent D of the power function. Moreover, one could interpret the result wrongly if one did not take into account a possible agglomeration of the nuclei. We have taken special precautions to avoid agglomeration and we obtained different results for the

just-treated sample and for one after several hours of relaxation. We believe that our results better reflect the reality of the object under study.

In this paper, neutron and small-angle scattering have been applied in a wide Q range in order to study the chromatin structure inside the HeLa nuclei. Firstly, we show the bi-fractal structure of the chromatin in the HeLa nuclei. Secondly, we identify the large-scale structure of the chromatin as being the logarithmic fractal, similar to that within the chicken erythrocyte nuclei. Note that the spatial range of the logarithmic fractal is an order of magnitude larger in the HeLa nucleus than in the chicken erythrocyte. Thirdly, we follow the process of agglomeration of nuclei over time, which may clearly influence the results of the ultra-SANS/SAXS and SESANS studies, if one does not take any preventive actions to keep the nuclei in the solvent separated.

2. Materials and methods

2.1. Sample preparation

The HeLa cells were grown in a cell culture flask (Orange Scientific) at $T = 310$ K with DMEM/F12 solution (Biolot, Russia) with added 10% fetal bovine serum (Biolot, Russia). They were removed from the substrate with a Versene/trypsin solution 1:1 (10 min) and washed by centrifugation for 5 min at 1000 r min^{-1} . The sediment of the cells was resuspended with a 10 ml Versene solution and centrifuged for 5 min. The acquired sediment of the cells was resuspended again with DMEM/F12 containing 15 mM HEPES solution and additionally with non-ionic detergent Triton X-100 (0.1%). The cells were lysed for 3–5 min, with periodical stirring of the suspension at room temperature. The processes of destruction of cells and separation of the nuclei were controlled by microscopy. The cell nuclei were fixed by 0.5% glutar aldehyde for 10 min and subsequently washed by centrifugation (three times) to remove the fixation agent with Versene solution for 10 min at 1000 r min^{-1} .

2.2. Flow cytometry

Flow cytometry is a method that measures the physical characteristics of a single particle. The principle of the method is simple: particles (cells or nuclei) flow in a fluid stream

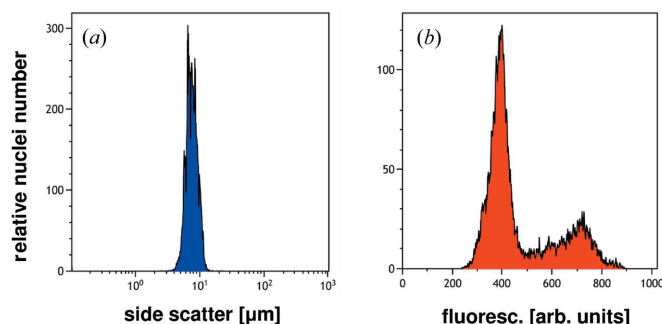


Figure 1
Flow cytometry histograms for the sample of the HeLa nuclei.

through a laser beam and scattering light is detected. The typical characteristics measured are the particle's relative size and relative fluorescence intensity. A flow cytofluorimeter (Cell Lab QUANTA SC by Beckman Coulter) was used to study the properties of the nuclei. As shown in Fig. 1(a) the average size of the nucleus is determined to be 7 μm . The DNA in the nuclei was stained to a concentration of 20 $\mu\text{g ml}^{-1}$ ethidium bromide, so that flow cytometry was able to distinguish between the nuclei in the different phases of the cell cycle. The higher peak of the fluorescence intensity corresponds to the interphase (G1), while fluorescence detected at the lower peak relates to the other phases. Fig. 1(b) shows clearly that 70% of nuclei are fixed in the G1 phase. These facts confirm that the nuclei are a monodisperse system and that the largest part of the nuclei are in the interphase.

2.3. SANS

The SANS method provides information about the density distribution in the object of interest, though in the Fourier (reciprocal) space. More generally, the scattering methods measure the Fourier transform of the correlation function $\gamma(r)$:

$$\gamma(r) = \left\langle \int_{\mathbb{R}^3} \rho(\mathbf{r}') \rho(\mathbf{r}' + \mathbf{r}) \, d\mathbf{r}' \right\rangle, \quad (1)$$

where $\rho(\mathbf{r})$ is the scattering density of the sample and the angled brackets stand for averaging over orientations. From the intensity of the scattering experiment one can recover the density–density correlation function but not the density variations themselves.

Nevertheless, SANS is one of the most informative techniques for studying the structure of matter at above-atomic scales from a few nanometres to a few micrometres. The intensity of neutron scattering $I(Q)$ measured in the experiment can be converted to the correlation function of the object $\gamma(r)$:

$$\gamma(r) = \frac{1}{2\pi} \int_0^\infty I(Q) \frac{\sin(Qr)}{Qr} Q^2 \, dQ. \quad (2)$$

The SANS study of the structural chromatin organization of the isolated HeLa nuclei was carried out in the momentum transfer range $[2 \times 10^{-2} - 3.4 \times 10^0] \text{ nm}^{-1}$ at the D11 instrument (ILL, Grenoble, France). The very small angle neutron scattering measurements were performed in the momentum transfer range $[1.5 \times 10^{-3} - 2 \times 10^{-2}] \text{ nm}^{-1}$ at the instrument KWS-3 [Heinz Maier-Leibnitz Zentrum (MLZ), Munich, Germany]. KWS-3 is a pinhole geometry machine which allows the detection of ultra-small scattering angles by using a double-focusing toroidal mirror. The same sample was used in performing both experiments. In order to achieve the maximum contrast, the nuclei of the cells were placed in heavy water D_2O with a concentration of more than 95%. Thus, as well as maximally increasing the neutron scattering intensity, we used the densest solution possible for these samples. The thickness of the sample was chosen to be 1 mm.

2.4. SESANS

To confirm the unusual fractal properties of DNA packaging on the large (1 μm) scale, the technique of SESANS was used. SESANS allows inhomogeneities to be studied on scales from 20 nm up to 20 μm (Rekvelde, 1996; Rekvelde *et al.*, 2005). This method gives reliable information on the correlation length of the object, which sometimes cannot be determined by the conventional SANS technique because of the resolution limitations.

In the SESANS technique the phenomenon of Larmor precession of the neutron magnetic moment in a magnetic field is employed to decode the scattering angle in the interaction of neutrons with the particle (Rekvelde *et al.*, 1996). The polarization of the neutron beam is measured as it passes through the sample. We perform the scan along the spatial coordinate z , which is perpendicular to the direction of the neutron beam, called the spin-echo length (SE length). The measured polarization $P(z)$ depends on the mesostructure of the sample and is described as follows (Rekvelde *et al.*, 2005):

$$P(z) = \exp\{l\sigma[G(z) - 1]\}, \quad (3)$$

where l is the thickness of the sample, σ is the total neutron cross section of the sample and $G(z)$ is the SESANS correlation function for the object. For isotropic systems, the function $G(z)$ is connected with the spatial correlation function $\gamma(r)$ via the Abel transformation (Andersson *et al.*, 2008):

$$\gamma(r) = -\frac{\xi}{\pi} \int_r^\infty \frac{G'(z)}{(z^2 - r^2)^{1/2}} \, dz. \quad (4)$$

The sample of the isolated HeLa nuclei (the same as for SANS) was investigated at the SESANS instrument of the Delft University of Technology, The Netherlands, in a range of scales $[3 \times 10^2 - 10^4] \text{ nm}$. The SESANS instrument uses a constant wavelength $\lambda = 2 \text{ \AA}$. The measurements were carried out in a solution of $\text{D}_2\text{O} > 95\%$ to reach the maximum contrast for the scattering. The thickness of the sample used in the SESANS experiment is equal to 4 mm.

3. Results and discussion

3.1. Inter-nuclei structure of HeLa in phosphate-buffered saline (PBS) buffer: SANS study

Typical images of the HeLa nuclei are shown in Fig. 2. A confocal microscope (Leica TSC SP5) was used to obtain these images. To obtain better visualization of the DNA, the nuclei were stained with Hoechst 33342 dye at a concentration of 1 $\mu\text{g ml}^{-1}$ [Figs. 2(a) and 2(c)]. The nuclei are well separated from one another. Note that the HeLa nuclei tend to agglomerate within several hours. Nevertheless, the agglomerations of nuclei can be redistributed into the solution of the isolated nuclei by pushing the agglomerates through a thin syringe.

The combined results of ultra-small-angle neutron scattering and SANS experiments are shown in Fig. 3. The SANS intensity is described by a power function $I(Q) \sim Q^{-D}$ with

the power $D = 2.41 \pm 0.01$ in the range $[8 \times 10^{-2} - 7 \times 10^{-1}] \text{ nm}^{-1}$. This power dependence demonstrates the fractal organization of the chromatin in the nucleus, with a dimension equal to the power $D_F = 2.41$. The intensity of the neutron scattering has a different power dependence in the momentum transfer range $[1.5 \times 10^{-3} - 8 \times 10^{-2}] \text{ nm}^{-1}$. It is well described by the expression

$$I(Q) = \frac{A}{[1 + (Q\xi)^2]^{D/2}} \quad (5)$$

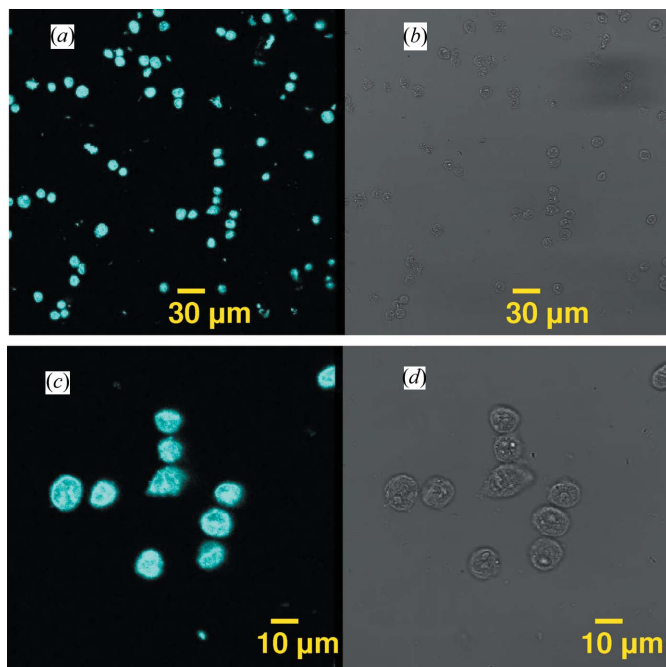


Figure 2 Confocal microscope images showing the isolated HeLa nuclei. (a), (c) Images of fluorescence of Hoechst 33342 DNA dye in HeLa nuclei. (b), (d) Images of HeLa nuclei.

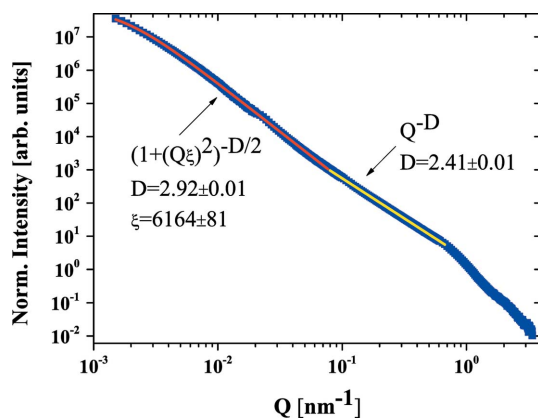


Figure 3 SANS on nuclei of HeLa. Lines represent data fits to the power law with two different exponents. The data for the intensity of neutron scattering in the momentum transfer range $[1.5 \times 10^{-3} - 8 \times 10^{-2}] \text{ nm}^{-1}$ were obtained at the KWS-3, MLZ, Munich, Germany. The data for the intensity of neutron scattering in the momentum transfer range $[8 \times 10^{-2} - 7 \times 10^{-1}] \text{ nm}^{-1}$ were obtained at the D11 instrument at ILL, Grenoble, France.

with the power $D = 2.92 \pm 0.01$, which accounts for the finite size of the nuclei $\xi = 6160 \pm 80 \text{ nm}$. The difference between the indexes observed in the different Q ranges allows one to conclude that the fractal structure of the chromatin in the nucleus changes its nature upon transition from the smaller scale (tens of nanometres) to the larger scale (hundreds of nanometres).

The correlation function of the object characterized by the scattering law of $[1 + (Q\xi)^2]^{-D/2}$ (in the case $Q\xi \gg 1, Q^{-D}$), with $2 < D < 3$, corresponds to a mass fractal of dimension D and is described by the expression $\gamma(r) \sim (r/\xi)^{D-3}$. With D approaching 3, the correlation function changes its nature and can be described by the ratio $\gamma(r) \sim \ln(\xi/r)$. The change in the nature of the correlation function leads to a fundamental change of the properties and structure of chromatin in the cell nucleus.

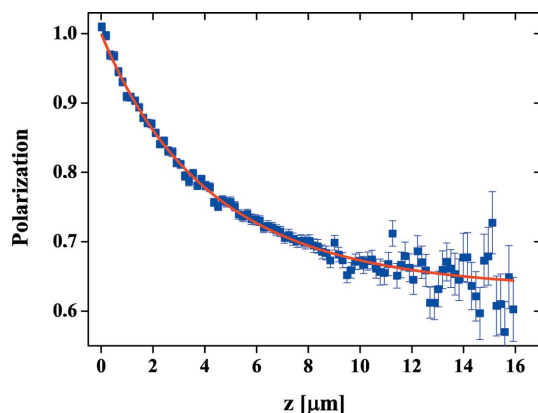
The bi-fractal structure of the chromatin in the HeLa nuclei is similar to the bi-fractal structure of the chromatin in chicken erythrocyte nuclei (Iashina *et al.*, 2017). Interestingly, the crossover point Q_{cp} from the volume fractal to the logarithmic fractal regimes is one order of magnitude larger for the HeLa nuclei ($Q_{cp} = 8 \times 10^{-2} \text{ nm}^{-1}$) than for the chicken erythrocyte ($Q_{cp} = 10^{-2} \text{ nm}^{-1}$). Moreover there is other evidence of chromatin bi-fractality. For instance, nuclear rheology demonstrated the fractal architecture of euchromatin and heterochromatin with different fractal dimensions $D_F = 2.6$ and $D_F = 2.2$, respectively (Bancaud *et al.*, 2012). We tend to the following explanation. On the small scale the diffusion of small molecules and nuclear proteins is very important to search for a specific target site in the DNA sequence; thus chromatin has a regular isotropic fractal structure with dimension $D_F = 2.4$ which is associated with DLA or percolation clusters. On the large scale the chromatin has a logarithmic fractal structure which is more compact than the volume fractal and the surface of the logarithmic fractal is present at all length scales (Iashina & Grigoriev, 2017). In other words the logarithmic fractal has a hierarchically branched structure which ensures the maximum availability of any section from the outside and the most compact, dense structure. We cannot exactly interpret the deep scaling (two orders of magnitude) of the logarithmic fractal in the HeLa cells. This should be a subject for forthcoming studies. However, we assume that the deep scaling of the logarithmic fractal is due to the high vital activity of the HeLa cells. In contrast to chicken erythrocyte nuclei which are synthetically inactive nuclei, HeLa nuclei divide quickly and often.

3.2. Inter-nuclei structure of HeLa in PBS buffer: SESANS study

Fig. 4 presents the normalized polarization P/P_0 as a function of the SE length z . We have found that the SESANS function of isolated HeLa nuclei is well described by

$$G(z) = \exp(-z/\xi), \quad (6)$$

where $\xi = 5.1 \pm 0.1 \mu\text{m}$ is the size of the nucleus. The exponential decay of the SESANS function indicates that the HeLa


Figure 4

Normalized SESANS polarization P as a function of the SE length z from the isolated HeLa nuclei. The line represents the fit $\exp\{\sigma l / [\exp(-z/\xi) - 1]\}$, with $\sigma l = 0.459 \pm 0.006$ and $\xi = (5.1 \pm 0.1) \times 10^3$ nm.

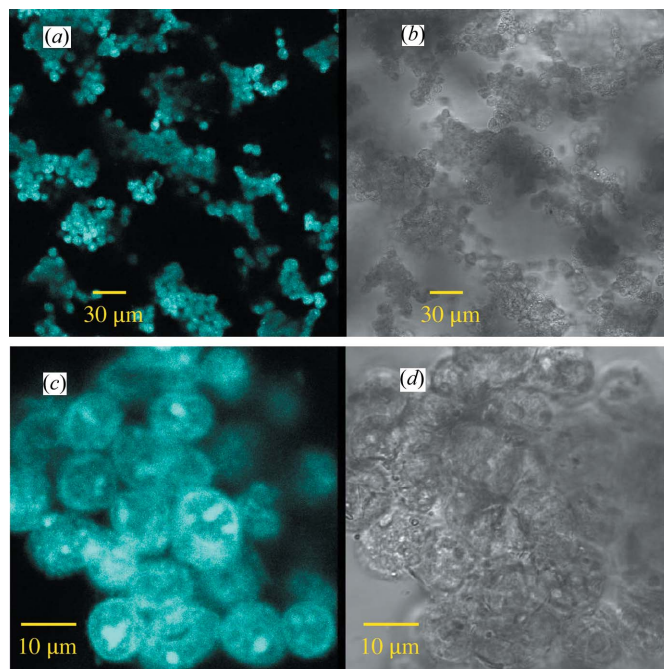
nucleus has a logarithmic correlation function $\gamma(r) \sim \ln(\xi/r)$ on the micrometre scale (Iashina *et al.*, 2017). Thus, the findings of the SESANS experiment support the conclusions derived from the SANS experiment. This means that the normal metric of the density distribution of the chromatin in HeLa nuclei is the logarithmic metric or ultrametric space on appropriate distances (Olemskoi & Flat, 1993).

3.3. Intra-nuclei structure of HeLa in PBS buffer: SANS study

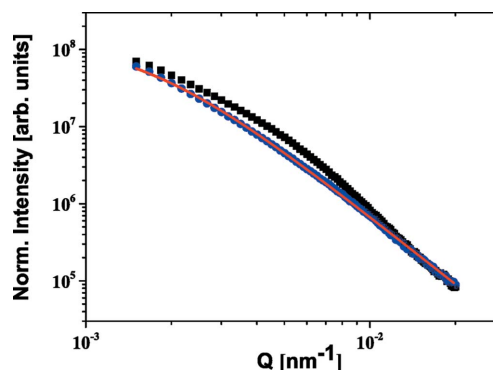
As noted already, the HeLa nuclei tend to agglomerate within several hours. Typical images of the agglomerated HeLa nuclei are shown in Fig. 5. For better visualization of the DNA, the nuclei were stained with Hoechst 33342 dye at a concentration of $1 \mu\text{g ml}^{-1}$ [Figs. 5(a) and 5(c)]. The agglomeration of the HeLa nuclei looks quite typical, like a bunch of grapes. However, as will be shown below, nuclei within this agglomeration do not just touch but penetrate deeply inside each other. Note that the structure of each nucleus does not change upon agglomeration because the nuclei were fixed by glutaraldehyde (see Section 2.1).

The SANS spectra from the isolated and agglomerated HeLa nuclei in the range of very small momentum transfer values are shown in Fig. 6. The data were obtained at the KWS-3, MLZ, Munich, Germany. The curve from the agglomerated HeLa nuclei demonstrates a small swelling which disappears after the sample is passed through a syringe. It is important to note that the agglomeration of nuclei can change the profile of the scattering cross section and thus may affect the index D of the power function [equation (5)], particularly in the very small Q range. Fig. 6 demonstrates clearly how much the Q dependence of the scattering intensity for isolated nuclei may be deformed upon agglomeration. Thus one should take all necessary measures to prepare the sample with isolated nuclei for study in ultra-SANS experiments.

In order to extract the changes occurring in the scattering intensity upon agglomeration of nuclei, we divided the scattering intensity into that from the agglomerated HeLa nuclei


Figure 5

Confocal microscope images showing the agglomerates of the HeLa nuclei. (a), (c) Images of fluorescence of Hoechst 33342 DNA dye in HeLa nuclei. (b), (d) Images of HeLa nuclei.


Figure 6

The momentum transfer dependence of the very small angle neutron scattering intensity from the isolated HeLa nuclei (blue points) and from the agglomerated HeLa nuclei (black points).

and that from the isolated ones (Fig. 7), thus obtaining the function attributed to the pair correlation between the nuclei. It can be seen as the structure factor of the agglomerated nuclei as soon as we notice a correlation peak (see Appendix A). However, the peak reveals the correlations on the distance of the order of $1 \mu\text{m}$, *i.e.* rather inside the nuclei than between them. This correlation peak in Fig. 7 can be described by the Lorentzian function in the log–lin scale,

$$L(Q) = A + \frac{B}{1 + [\ln(Q) - \ln(\kappa)]^2}, \quad (7)$$

with the centre in $\kappa = (5.5 \pm 0.3) \times 10^{-3} \text{ nm}^{-1}$, scale factor $B = 0.99 \pm 0.01$ and background constant $A = 0.439 \pm 0.003$.

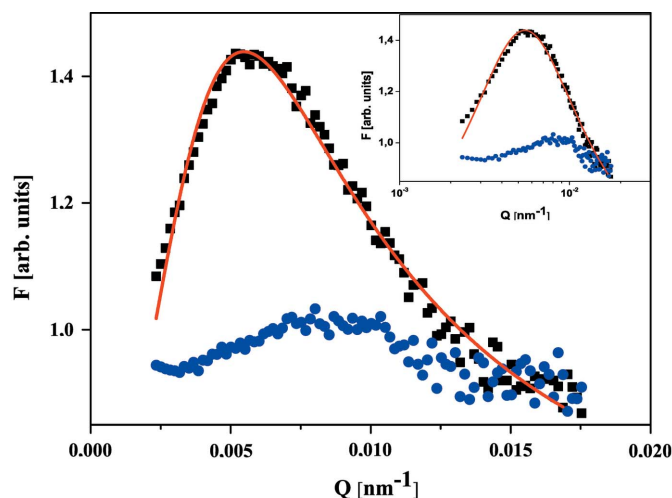


Figure 7
The ratio of the experimental SANS intensity from isolated HeLa nuclei to the curve with the best-fitted parameters [equation (5)] (blue points). The ratio of the experimental SANS intensity from agglomerated HeLa nuclei to the best-fitted curve for the isolated HeLa nuclei [equation (5)] (black points). Inset: same dependence on the log–lin scale.

Thus we show that the agglomeration of the HeLa nuclei with an external size of about 6.15 μm leads to correlations on a scale of the order of 1 μm . This observation shows that the HeLa nuclei interpenetrate each other upon agglomeration. It is especially interesting that the correlation is described by the peak function (Lorentzian) but on the logarithmic scale.

We further speculate that the Lorentzian logarithmically stretched along the coordinate should be closely associated with the logarithmic correlation function $\gamma(r) \sim \ln(\xi/r)$ of the nucleus on the scales from 6150 to 80 nm. In other words, should the objects with internal structure described by the logarithmic correlation function interpenetrate, they form the pair correlation function described by the Lorentzian on the logarithmic scale.

3.4. Intra-nuclei structure of HeLa in PBS buffer: SESANS study

The ability of the HeLa nuclei to agglomerate and, unusually, to interpenetrate is clearly observed in the SESANS experiments. We have conducted the same set of SESANS measurements for the sample passed through a syringe and for the same sample but 7 h later. All our experiments show that the sample after the procedure with the syringe consists of isolated nuclei but the nuclei should agglomerate (and interpenetrate) within 7 h. Fig. 8 presents the normalized polarization P as a function of the SE length z from the isolated HeLa nuclei (blue points) and the agglomerated HeLa nuclei (black points). As was shown above, the SESANS correlation function $G(z)$ for the isolated HeLa nuclei is well described by the exponential decay [see equation (3) and Fig. 4]. The change of the SESANS correlation function upon agglomeration can be considered in terms of the additional neutron scattering coming from the correlated nuclei. In this case the function related to the agglomeration

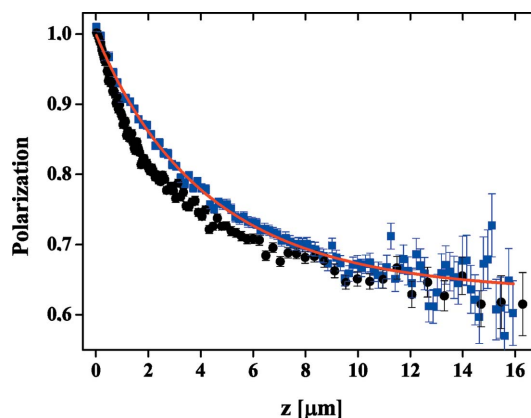


Figure 8
Normalized SESANS polarization P as a function of the SE length z from isolated HeLa nuclei (blue points) and agglomerated HeLa nuclei (black points). The line represents a fit $\exp\{\sigma[\exp(-z/\xi) - 1]\}$, with $\sigma = 0.459 \pm 0.006$ and $\xi = (5.1 \pm 0.1) \times 10^3$ nm.

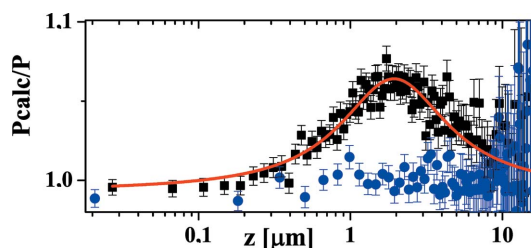


Figure 9
The ratio of the fitted polarization from isolated HeLa nuclei to the experimental polarization from isolated HeLa nuclei (blue points) and the ratio of fitted polarization from the isolated HeLa nuclei to the experimental polarization from agglomerated HeLa nuclei (black points). The black line represents a best fit with equation (6).

can be extracted by a division of one set of the data by the other (see Appendix A).

Fig. 9 presents the ratio of the fitted polarization from the isolated HeLa nuclei to the experimental polarization from agglomerated HeLa nuclei (black points). Thus the contribution to the SESANS function from the aggregated (interpenetrated) nuclei can be well approximated by the Lorentzian function on the logarithmic scale in real space:

$$L(z) = A + \frac{B}{1 + [\ln(z) - \ln(1/\kappa)]^2} \quad (8)$$

with the centre in $1/\kappa = 1.94 \pm 0.05 \mu\text{m}$, scale factor $B = 0.071 \pm 0.003$ and constant $A = 0.992 \pm 0.002$ (Fig. 9). The best-fit parameters show that the correlation function changes upon agglomeration only on a scale of the order of $1/\kappa \sim 2 \mu\text{m}$. We suppose that the nuclei interpenetrate upon agglomeration and the characteristic penetration depth reached is 2 μm while the size of the nucleus is equal to 5.1 μm . Moreover, the exponential SESANS function [equation (6)] corresponds to the logarithmic correlation function $\ln(\xi/r)$ of the HeLa nuclei on the micrometre scale and to the logarithmic character of the pair correlation peak function [equation (8)] in analogy to the SANS study.

4. Discussion

It is worthwhile discussing some features and results of the neutron experiments presented here. Firstly, as the nuclei were placed in heavy water and D₂O has filled chromatin-free space inside the nuclei, then the scattering intensity is caused by contrast between the chromatin and heavy water penetrating into the interchromatin voids at all scales from a few nanometres to several micrometres. In other words, neutrons are scattered from inhomogeneities formed by chromatin against a background scattering from heavy water. This means that the SANS and SESANS experiments give information about the internal structure (fractal architecture) of chromatin. One can invert this picture and consider the obtained results for the fractal architecture of the chromatin-free space, which is the medium available for diffusive movement. This inverted picture is favourable for understanding how the chromatin organization can influence the gene functioning and storage of genetic information (Bancaud *et al.*, 2012).

Secondly, the detected exponents in the power law of scattering intensity from the HeLa nuclei are similar to those from chicken erythrocyte nuclei (Iashina *et al.*, 2017), which supports the general hypothesis of the bi-fractal structure of chromatin in the interphase nuclei. The small-scale fractal level corresponds to a volume fractal with dimension $D_F = 2.41$, while the large-scale fractal level corresponds to a logarithmic fractal with correlation function $\gamma(r) \sim \ln(\xi/r)$. The volume fractal is self-similar at different scales, while the logarithmic fractal is hierarchically changed upon scaling (Iashina & Grigoriev, 2017). As a result the logarithmic fractal is more compact than the volume fractal, but it still has a rather high surface area, which provides accessibility at all length scales. Apparently, such bi-fractal chromatin organization is the result of an evolutionary process of optimizing the compactness and accessibility of gene packing. The small-scale volume fractal organization is built to satisfy the necessity of protein diffusion, while the large-scale logarithmic fractal is formed under the influence of two factors: protein diffusion and gene interaction.

Thirdly, the logarithmic fractal in the HeLa nuclei covers two orders of magnitude in scale while the volume fractal spreads for one order only. In the nuclei of the chicken erythrocytes it is exactly the opposite: the logarithmic fractal occurs within one order of the large-scale chromatin architecture but the volume fractal spreads for two orders of magnitude in scale. We assume that this difference is related to the fact that the chicken erythrocyte nucleus is dormant while the HeLa nucleus is actively dividing. It may also be due to epistasis: the nuclei that need more interactions between loci have a longer range of the logarithmic fractal. Detection of the cubic dependence of scattering intensity in a wide Q range is an additional argument for the existence of such a universal scattering mode for chromatin, which was assumed in previous work (Lebedev *et al.*, 2005; Iashina *et al.*, 2017) based on a restricted Q interval strongly affected by the nucleus size cut-off.

In the fourth place, the HeLa nuclei tend to agglomerate over time. The long-scale logarithmic fractal structure of the large-scale chromatin organization allows the HeLa nucleus to

penetrate deeply into the adjacent nucleus during the agglomeration process. The interpenetration phenomenon of the HeLa nuclei shows that the chromatin-free space of one nucleus is not negligible: it is as large as the volume occupied by the chromatin itself. Free space within the nucleus is needed, for example, for the process of DNA synthesis in order to allow two nuclei to form in the same volume. Interestingly it is the logarithmic fractal architecture of chromatin that provides a comfortable compartment for this most important function of the cell.

In the fifth place, the logarithmic correlation function corresponds to the logarithmic metric or the ultrametric space of the density distribution of chromatin in HeLa nuclei (Iashina *et al.*, 2017; Olemskoi & Flat, 1993). The ultrametric space is determined by the fact that, being a reflection of the hierarchical structure of the system, it realizes a so-called logarithmic metric for physically observable quantities (Olemskoi & Flat, 1993). The fact that the pair correlation function of the agglomerated nuclei is described by the peak function along the logarithmic coordinate also indicates that the interpenetration of nuclei occurs in the ultrametric space.

In the sixth place, as shown in the work of Iashina & Grigoriev (2017), the Fourier transform of equation (5) gives the correlation function that is described by the $(D - 3)/2$ -order modified Bessel function of the second kind multiplied by the power function $r^{(D-3)/2}$. The functions $(r/\xi)^{D-3}$ and $\ln(\xi/r)$ are asymptotics of this expression in the region of small r ($r/\xi < 1$): in other words, inside the nucleus in the case $2 < D < 3$ and $D = 3$, respectively. Since the correlation function is an analogue of the density, the particle volume can be obtained by integrating it over 3D space. As a finite particle size is taken into account in the correlation function, such a procedure requires no additional modification in order to take its boundary into account. The derived expression for the particle volume is proportional to $(D - 2)$. As a result, the space that is occupied by the logarithmic fractal with $(D = 3)$ is twice as small as 3D non-fractal object with $(D = 4)$.

5. Conclusion

Here, we offer the logarithmic fractal as a model of the large-scale organization of interphase chromatin and explain its biological significance with respect to DNA functions. The HeLa nucleus has a bi-fractal structure. The correlation function from 9 to 80 nm is a power function $\gamma(r) = r^{3-D}$, with $D = 2.41$. The power correlation function corresponds to the volume fractal structure with fractal dimension $D_F = 2.41$. The correlation function of the HeLa nucleus changes to the logarithmic function $\gamma(r) = \ln(r/\xi)$ ($\xi = 5100$ nm) on a scale from 80 to 5100 nm. We suppose that such a structure of the HeLa nuclei provides high accessibility, as a consequence of which the nuclei interpenetrate deeply into each other during the agglomeration process. We believe this phenomenon is related to the wide range of scales (two times more than for the chicken erythrocyte nucleus) of the logarithmic fractal in the HeLa nucleus.

APPENDIX A

The correlation function of interpenetrated nuclei can be written as follows:

$$\gamma(r) = \gamma_a(r) + \Delta\gamma(r), \tag{9}$$

where $\gamma_a(r)$ is the correlation function of isolated nuclei and $\Delta\gamma(r)$ is a contribution that describes the interpenetration phenomenon. The Fourier transform of the correlation function $\{\mathcal{F}[\gamma(r)]\}$ gives the neutron scattering intensity from interpenetrated nuclei $I(Q)$, which can be written as a product of two functions: the intensity from isolated nuclei and a function that describes the interpenetration phenomenon:

$$\begin{aligned} I(Q) &= \mathcal{F}[\gamma_a(r)] + \mathcal{F}[\Delta\gamma(r)] \\ &= I_a(Q) + I_\Delta(Q) = I_a(Q) \left[1 + \frac{I_\Delta(Q)}{I_a(Q)} \right], \end{aligned} \tag{10}$$

where $I_a(Q)$ is the scattering intensity of the individual scatterers and $I_\Delta(Q)$ is an additional intensity related to the interference between scattering waves coming from different scatterers. Thus, the total scattering cross section consists of two parts:

$$\sigma = \int_{\mathbb{R}} I(Q) dQ = \sigma_a + \sigma_\Delta. \tag{11}$$

The neutron scattering intensity $I(Q)$ is directly related to the SESANS function $G(z)$ as

$$G(z) = \frac{1}{\sigma k_0^2} \int_{\mathbb{R}^2} \cos(Q_z z) I(Q) dQ_y dQ_z, \tag{12}$$

where k_0 is the wavenumber of the incident neutrons. We rewrite the expression for the SESANS function using equations (8) and (10):

$$\begin{aligned} G(z) &= \frac{\sigma_a}{\sigma} \frac{1}{\sigma_a k_0^2} \int_{\mathbb{R}^2} \cos(Q_z z) I_a(Q) dQ_y dQ_z \\ &+ \frac{\sigma_\Delta}{\sigma} \frac{1}{\sigma_\Delta k_0^2} \int_{\mathbb{R}^2} \cos(Q_z z) I_\Delta(Q) dQ_y dQ_z. \end{aligned} \tag{13}$$

The first integral is the contribution to $G(z)$ of the single particle, otherwise known as the autocorrelation SESANS function $G_a(z)$. The second integral is the contribution to $G(z)$ from inter-particle interference, or the pair correlation SESANS function $G_\Delta(z)$,

$$G(z) = \frac{\sigma_a}{\sigma} G_a(z) + \frac{\sigma_\Delta}{\sigma} G_\Delta(z). \tag{14}$$

The expression for the polarization [equation (4)] can be written as follows:

$$\begin{aligned} P(z) &= \exp \left\{ \sigma l \left[\frac{\sigma_a}{\sigma} G_a(z) + \frac{\sigma_\Delta}{\sigma} G_\Delta(z) - 1 \right] \right\} \\ &= \exp [\sigma_a l G_a(z) + \sigma_\Delta l G_\Delta(z) - \sigma_a l - \sigma_\Delta l] \\ &= P(z)_a P(z)_\Delta. \end{aligned} \tag{15}$$

Thus, the simple division of the total polarization by the polarization corresponding to the scattering from the indi-

vidual particles gives the polarization related to the interference scattering.

Acknowledgements

The authors would like to thank E. V. Velichko for assistance rendered.

Funding information

Funding for this research was provided by Russian Foundation for Basic Research (grant No. 17-02-00313 A).

References

Alberts, B. (2008). *Molecular Biology of the Cell*. New York: Garland Science.

Almassalha, L. M., Tiwari, A., Ruhoff, P. T., Stypula-Cyrus, Y., Cherkezyan, L., Matsuda, H., Dela Cruz, M. A., Chandler, J. E., White, C., Maneval, C., Subramanian, H., Szleifer, I., Roy, H. K. & Backman, V. (2017). *Sci. Rep.* **7**, 41061.

Andersson, R., van Heijkamp, L. F., de Schepper, I. M. & Bouwman, W. G. (2008). *J. Appl. Cryst.* **41**, 868–885.

Bale, H. & Schmidt, P. (1984). *Phys. Rev. Lett.* **53**, 596–599.

Bancaud, A., Lavelle, Ch., Huet, S. & Ellenberg, J. (2012). *Nucleic Acids Res.* **40**, 8783–8792.

Bénichou, O., Chevalier, C., Meyer, B. & Voituriez, R. (2011). *Phys. Rev. Lett.* **106**, 038102.

Bintu, L., Ishibashi, T., Dangkulwanich, M., Wu, Yu.-Y., Lubkowska, L., Kashlev, M. & Bustamante, C. (2012). *Cell*, **151**, 738–749.

Blossey, R. (2017). *Chromatin: Structure, Dynamics, Regulation*. New York: Chapman and Hall/CRC.

Boettiger, A. N., Bintu, B., Moffitt, J. R., Wang, S., Beliveau, B. J., Fudenberg, G., Imakaev, M., Mirny, L. A., Wu, Ch. & Zhuang, X. (2016). *Nature*, **529**, 418–422.

Dekker, J., Rippe, K., Dekker, M. & Kleckner, N. (2002). *Science*, **295**, 1306–1311.

Feder, J. (1998). *Fractals*. New York: Plenum.

Grosberg, A., Rabin, Y., Havlin, S. & Neer, A. (1993). *Europhys. Lett.* **23**, 373–378.

Grosberg, A. Yu., Nechaev, S. K. & Shakhnovich, E. I. (1988). *J. Phys. Fr.* **49**, 2095–2100.

Iashina, E. G. & Grigoriev, S. V. (2017). *J. Surf. Invest.* **11**, 897–907.

Iashina, E. G., Velichko, E. V., Filatov, M. V., Bouwman, W. G., Duif, C. P., Brulet, A. & Grigoriev, S. V. (2017). *Phys. Rev. E*, **96**, 012411.

Joti, Ya., Hikima, T., Nishino, Y., Kamada, F., Hihara, S., Takata, H., Ishikawa, T. & Maeshima, K. (2012). *Nucleus*, **3**, 404–410.

Lajoie, B. R., Dekker, J. & Kaplan, N. (2015). *Methods*, **72**, 65–75.

Lebedev, D. V., Filatov, M. V., Kuklin, A. I., Islamov, A. Kh., Kentzinger, E., Pantina, R., Toperverg, B. P. & Isaev-Ivanov, V. V. (2005). *FEBS Lett.* **579**, 1465–1468.

Lieberman-Aiden, E., van Berkum, N. L., Williams, L., Imakaev, M., Ragozcy, T., Telling, A., Amit, I., Lajoie, B. R., Sabo, P. J., Dorschner, M. O., Sandstrom, R., Bernstein, B., Bender, M. A., Groudine, M., Gnirke, A., Stamatoyannopoulos, J., Mirny, L. A., Lander, E. S. & Dekker, J. (2009). *Science*, **326**, 289–293.

Mandelbrot, B. (1983). *The Fractal Geometry of Nature*. New York: Freeman.

Martin, J. E. & Hurd, A. J. (1987). *J. Appl. Cryst.* **20**, 61–78.

Miglani, G. S. (2006). *Developmental Genetics*. New Delhi: I. K. International Pvt Ltd.

Mirny, L. A. (2011). *Chromosome Res.* **19**, 37–51.

Misteli, T. (2007). *Cell*, **128**, 787–800.

- Olemskoi, A. I. & Flat, A. Y. (1993). *Usp. Fizicheskikh Nauk.* **163**, 1.
- Ou, H. D., Phan, S., Deerinck, Th. J., Thor, A., Ellisman, M. H. & O'Shea, C. C. (2017). *Science*, **357**, 6349.
- Rekveltdt, M. T. (1996). *Nucl. Instrum. Methods Phys. Res. B*, **114**, 366–370.
- Rekveltdt, M. T., Plomp, J., Bouwman, W. G., Kraan, W. H., Grigoriev, S. V. & Blaauw, M. (2005). *Rev. Sci. Instrum.* **76**, 033901.
- Teixeira, J. (1988). *J. Appl. Cryst.* **21**, 781–785.
- West, G. B., Brown, J. H. & Enquist, B. J. (1999). *Science*, **284**, 1677.
- Widom, J. & Klug, A. (1985). *Cell*, **43**, 207–213.
- Wolffe, A. (1999). *Chromatin: Structure and Function*, 3rd ed. San Diego: Academic Press.
- Woodcock, C. L., Grigoryev, S. A., Horowitz, R. A. & Whitaker, N. (1993). *Proc. Natl Acad. Sci. USA*, **90**, 9021–9025.
- Yi, J., Stypula-Cyrus, Y., Blaha, C. S., Roy, H. K. & Backman, V. (2015). *Biophys. J.* **109**, 2218–2226.